High yield production of 2-methyltetrahydrofuran biofuel with reusable Ni-Co catalysts

Emilia Soszka, Marcin J drzejczyk, Nicolas Keller, Agnieszka Ruppert

High yield production of 2-methyltetrahydrofuran biofuel with reusable Ni-Co catalysts

Emilia Soszka[1], Marcin Jędrzejczyk[1], Nicolas Keller[2], Agnieszka M. Ruppert[1*]

[1] Institute of General and Ecological Chemistry, Lodz University of Technology, ul. Żeromskiego 116, 90-924 Łódź (Poland)

[2] Institut de Chimie et Procédés pour l'Energie, l'Environnement et la Santé, CNRS/University of Strasbourg, 67087 Strasbourg, France ; nkeller@unistra.fr

*Correspondence: agnieszka.ruppert@p.lodz.pl

ABSTRACT

The sustainable production of environmentally-friendly alternative fuels from renewable resources is one of the worldwide high-prospect strategies for future biorefinery schemes. 2-methyltetrahydrofuran (2-MTHF) that can be obtained from renewable sources such as lignocellulosic biomass is considered as an ideal green fuel competitive to benchmarks products due to high-value properties like high energy density. In our work we showed that bimetallic Ni-Co/γ-Al_2O_3 catalysts with an appropriate amount of Ni are worth robust, reusable and cheap earth-abundant non-noble metals-based catalysts enabling the high yield production of 2-MTHF. The factors allowing the activity to be strongly boosted compared to the monometallic counterparts while keeping a high selectivity to the targeted 2-MTHF product were identified and discussed. Among the key factors we identified the role of the Ni-Co interaction allowing the Ni availability at the surface of the catalyst to be enhanced. Additionally, the surface acidity was recognized as another important factor. Silica supported catalysts were selective towards

the 1,4-pentanediol (1,4-PDO) intermediate obtained by GVL dehydration, while more acidic γ-Al_2O_3 was pushing the reaction further towards 2-MTHF. The synthesis parameters were optimized in terms of reduction temperature (500°C) and Ni:Co ratio (1:4) on the most active γ-Al_2O_3 supported catalyst.

KEYWORDS: sustainable furanic fuel, 2-methyltetrahydrofuran, gamma-valerolactone, Ni-Co catalysts,

1. INTRODUCTION

The sustainable production of environmentally-friendly alternative fuels out of renewable bioresources is one of the high-prospect strategies for future biorefinery schemes. In this respect, 2-methyltetrahydrofuran (2-MTHF) can be considered as an ideal green fuel alternative of high value, as it can be obtained from renewable sources such as lignocellulosic biomass and shows advanced applications in fuel industry [1,2]. It is a promising sustainable fuel, competitive with benchmarks products like ethanol or bio-derived γ-valerolactone (GVL), due to its high energy density and very low water solubility [3], while it can be easily blended with gasoline up to 70% [4]. Additionally, it is considered as a bio-derived solvent with low miscibility with water, excellent stability, high boiling point and easy biodegradability which makes it a very attractive and competitive sustainable product for fuel industry [5,6,7].

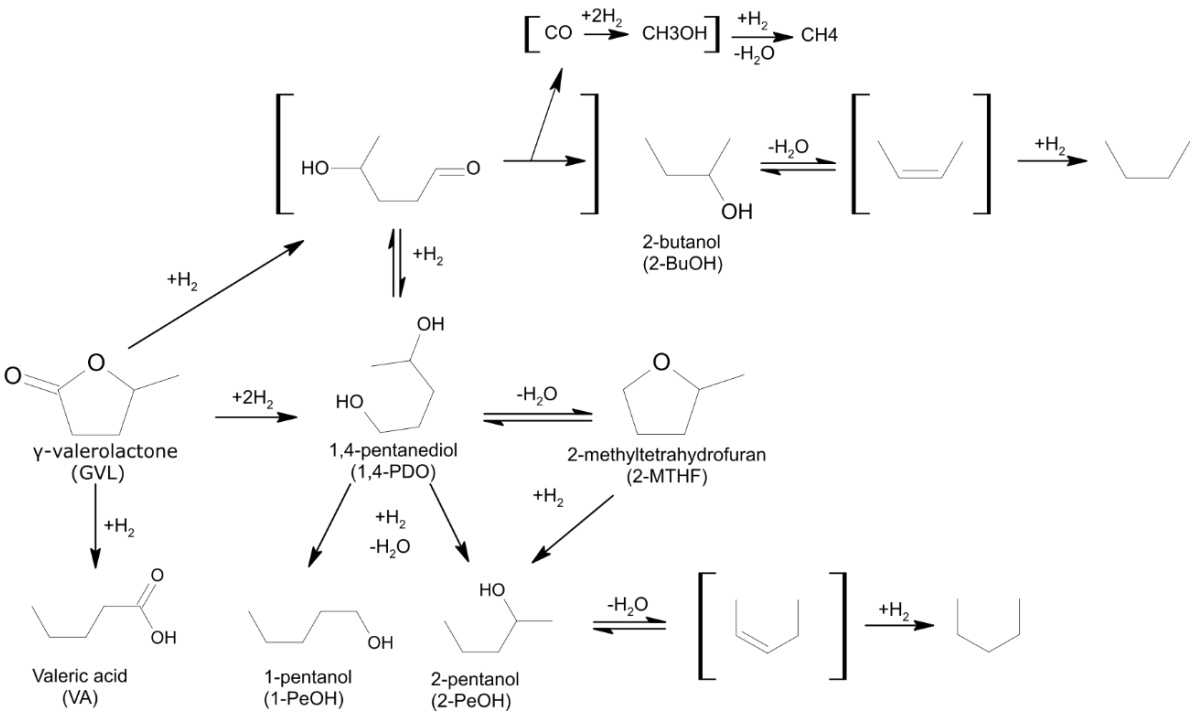

Scheme 1. Overall reaction pathways of the stepwise hydrodeoxygenation of GVL into 2-MTHF

2-MTHF is derived from lignocellulosic biomass via a multi-step sequential process, consisting first in the hydrolysis of cellulose towards levulinic acid (LA), and its subsequent hydrogenation towards GVL, that can occur easily even in mild reaction conditions [8,9]. The production of GVL from biomass-derived levulinic acid is already a well-studied step with optimized catalysts [8,9]. Therefore it is highly worth to investigate the following step in the biomass-value chain towards biofuels, that is usually more demanding. It corresponds to the hydrogenolysis of the GVL ester bond to form the 1,4-pentanediol (1,4-PDO) intermediate, that can be further dehydrated into 2-MTHF (scheme 1) [10]. The endergonic nature (ΔG^0 = 70 kJ mol^{-1} at 250°C) of the GVL conversion into 1,4-PDO usually requests severe reaction conditions such as high temperature and pressure [11]. Chemically-speaking, this first hydrogenation step requires breaking the C–O bond, and hydrogenating the cyclic ester. This two-step sequence of cyclic ester bond hydrogenolysis and further cyclisation is part of a complex reaction network with multiple competing side steps. A suited catalyst design is therefore crucial, and the catalysts should possess well-balanced surface sites combining the opening of the GVL ring with both hydrogenation and dehydration functions for achieving high MTHF yields while maintaining high selectivity features, notably by avoiding further hydrogenation of the 1,4-PDO intermediate towards diols (like 1-PeOH, 2-PeOH or 2-BuOH). Table S1 summarizes some recent representative works from the literature.

The use of earth-abundant non-noble metals as substitutes to noble metals as catalysts is now a current global strategy resulting from the vital necessity of lowering the environmental impacts and of considering global resource sustainability aspects. Among them, Cu was often highlighted as an efficient metal allowing high selectivity to 2-MTHF or 1,4-PDO to be achieved in relatively mild conditions. However high metal loadings were usually required [12].

An elegant approach allowing the properties of the catalysts to be tuned in order to boost its performances is based on the use of dopants or of bimetallic systems. Ni-Cu catalysts supported on Al_2O_3 were shown in the work of Obregón et al. to give a high yield 2-MTHF of 64% at 230°C and an H_2 pressure of 50 bar [13]. Despite a promising activity, the catalysts deactivated during reusability cycling tests due to carbon deposition.

Much lower interest has been given to other transition metals such as Co, as monometallic or bimetallic catalysts. However, suited reaction conditions (temperature and H_2 pressure) allowed Novodárszki et al. [14] to use recently Co/SiO_2 catalysts for performing selectively the solvent-free hydrodeoxygenation of levulinic acid into 2-MTHF with maximum yield of 70% for a Co loading of 8%, the activity being strongly influenced by the temperature. Lastly, we showed that the activity of Co/TiO_2 catalysts is highly depending on the features of the TiO_2 support in the hydrogenation of GVL into 2-MTHF [15]. We demonstrated the beneficial co-presence of both anatase and rutile crystalline phases within the TiO_2 support, and we proposed that the crystalline phase nature is not only influencing key-factors such as the Co particle size and the catalyst acidity, but also allows the SMSI effect to be tuned for achieving optimum performances in the synthesis of 2-MTHF.

Among bimetallic Co-based systems, supported Ni-Co catalysts are receiving a growing interest for various reactions, and in particular for hydrogenation reactions from biomass-derived substrates [16,17]. 2%Ni-20%Co/C catalyst allowed notably a high-yield of dimethylfuran production (95%) to be obtained from hydroxymethylfurfural under mild conditions (130°C, 1 MPa H_2) [18]. The high activity and stability reported were proposed to originate from the synergistic effect between Ni and CoO_x species, and from a stabilizing effect of Ni on CoO_x, respectively. Li et al. attributed the high yield to tetrahydrofurfuryl alcohol obtained from furfural substrate to a synergistic effect between Ni^0, CoO and spinel $NiCo_2O_4$ phases [17]. They suggested that the $NiCo_2O_4$ spinel in appropriate amount enhanced

reducibility of Ni catalysts in the presence of Co, and favored an even and high dispersion of both Ni^0 and CoO active sites by inhibiting the crystallite growth over the short-channeled SBA-15 used as support. On another hand, Kondeboina et al. suggested that the formation of a surface alloy was responsible for both the enhanced coke resistance capacity and the high activity of a NiCo/γ-Al_2O_3 catalyst in the C=O hydrogenation reaction from ethyl levulinate to GVL, which makes it a very promising catalyst [19].

Therefore, the aim of the current work was to investigate the ability of novel supported NiCo catalysts to boost performances in the production of the furanic 2-MTHF biofuel. To this end, the potential of NiCo catalysts supported on a selection of metal oxide supports of interest, namely TiO_2, γ-Al_2O_3 and SiO_2, was demonstrated. We studied to which extent the 2-MTHF production was influenced by the main physico-chemical properties of a novel supported NiCo catalysts for deriving the key-factors responsible for the catalyst performances.

2. EXPERIMENTAL

2.1. Material and Chemicals

$Ni(NO_3)_2x6H_2O$ (100% pure, Chempur, Poland) and $Co(NO_3)_2x6H_2O$ (99.9%, Eurochem, Poland) were used as received, as well as γ-valerolactone (99%, Sigma Aldrich) and 1,4-dioxane (98% pure, POCH, Poland). Anatase-rutile mixed phase Aeroxide© TiO_2 (P25) was delivered by Evonik-Degussa (Germany). SiO_2 (silica gel 60) and γ-Al_2O_3 (type 507 C Neutral) were purchased from Merck (Germany) and Fluka (Switzerland), respectively.

2.2. Catalyst preparation

Bimetallic 1%Ni-4%Co catalysts were prepared on the different supports following the wet impregnation method using $Ni(NO_3)_2$•$6H_2O$ and $Co(NO_3)_2$•$6H_2O$ as metal precursors in water.

After the solvent evaporation, the catalysts were dried at 120°C for 2 h, calcined at 500°C for 5 h under a flow of air with a temperature ramp rate of 5°C/min. The samples were cooled down to room temperature and further reduced under H_2 flow for 1 h at 500°C (25°C/min).

2.3.Characterization techniques

Temperature-programmed reduction (TPR)

Temperature-Programmed Reduction (TPR) was carried out on the AMI1 system (Altamira Instr., Pittsburgh, PA, USA) using a thermal conductivity detector for studying the catalyst reducibility. TPR was performed on the samples after the calcination step. The TPR profiles were recorded with a 10°C/min heating rate, using a mixture of 5 vol.% H_2 and 95 vol.% Ar at a space velocity of 3.1 x 10^{-9} g s^{-1} cm^{-3}.

Temperature-Programmed Desorption (TPD) of NH_3 was performed for studying the catalyst acidity. The NH_3-TPD experiments were implemented in a home-made quartz-based flow micro-reactor. Before all experiments, the surface of the catalyst was cleaned under He flow for 30 min at 500°C. The catalyst was then cooled down to 100°C, and NH_3 was adsorbed on the surface of the catalyst for 15 min at 100°C. Prior to measurement, physically-adsorbed NH_3 was removed from the surface of the catalyst by He flow cleaning for 15 min before cooling down the sample to the ambient temperature. The NH_3-TPD experiment was performed from room temperature to 500°C with a 25°C/min heating rate.

X-ray diffraction (XRD) measurements were performed on a PANalyticalX'Pert Pro MPD diffractometer (Malvern PANalytical, Malvern, United Kingdom), using a Cu long-fine focus XRD tube working at 30 mA and 40 kV as an X-ray source. Data were recorded in the 2θ mode with a 0.0167° step. Crystalline phases were identified by referring to the ICDD PDF-2 database (version 2004).

Time-of-Flight Secondary Ion Mass Spectrometry (ToF-SIMS) measurements were carried out in a TOF-SIMS IV instrument (ION-TOF GmbH) equipped with a 25 kV pulsed Bi_3^+ primary ion gun in static mode. The analyzed area of the sample surface was 500 μm x 500 μm. During the analysis, a pulsed low-energy electron flood gun was used for charge neutralization. The number of counts of selected ions from the mass spectra was normalized on the basis of the total ion count for allowing semi-quantitative analysis.

X-Ray Photoelectron Spectroscopy (XPS) characterization was performed on a ThermoVG MultilabESCA3000 spectrometer equipped with an Al Kα anode (hλ = 1486.6 eV). The energy shift due to electrostatic charging was subtracted using the contamination sp^2 carbon C 1s band at 284.6 eV. Contributions with Doniach–Sunjic shape [20] and a S-shaped Shirley type background [21] were used. The surface atomic ratios were obtained using the appropriate experimental sensitivity factors, as determined by Scofield [22].

2.4.Catalytic tests

The catalysts were tested in the γ-valerolactone (GVL) hydrogenation in high pressure reaction conditions. The activity tests were performed in liquid phase using 1,4-dioxane as solvent within a 100 mL stainless-steel reactor (Parr, Germany). The reactions were carried out with 1 g of GVL, 0.6 g of catalyst and 30 mL of 1,4-dioxane. The reactor was flushed with hydrogen to remove air and the reactor was pressurized with hydrogen to 50 bar before the reaction was performed at 230°C for 5 h with a stirring rate of 800 rpm. The reaction conditions were chosen for obtaining conversion levels allowing for a valid comparison of the catalyst performances, in agreement with the literature. The reactor was further cooled down and the pressure was released. The obtained reaction mixture was centrifuged to separate the catalyst from the solution. The liquid products were analyzed using an external standard on an Agilent

7820A GC instrument equipped with a CP-Wax 52 CB capillary column and a flame ionization detector.

GVL elimination, GVL conversion and product yields were calculated as follows:

$$Elimination\ (GVL) = \frac{n_{GVLi} - n_{GVLr}}{n_{GVLi}} \times 100\%$$

$$Yield\ (prod) = \frac{n_{prod}}{n_{GVLi}} \times 100\%$$

$$Conversion\ (GVL) = \frac{\sum n_{prod}}{n_{GVLi}} \times 100\%$$

n_{GVLi} and n_{GVLr} being the number of moles of GVL molecules before and after the reaction, respectively, and n_{prod} being the number of moles of a given product in the reaction mixture. For recycling tests, the catalyst was washed with dioxane before use in the next cycle.

3. RESULTS AND DISCUSSION

3.1. Characterization of the Ni-Co catalysts

The main physico-chemical properties of the TiO_2, SiO_2 and Al_2O_3 supported Ni-Co catalysts are summarized in Table 1, and the XRD patterns of the catalysts are shown in Figure 1. The characteristic signature of the TiO_2, Al_2O_3 and SiO_2 supports was recorded. All the reflexes were indexed in the I41/amd and P42/mnm tetragonal unit cells of the anatase and rutile TiO_2 polymorphs or corresponded to the main diffraction peaks at 2θ 37.54° (311), 45.67° (400) and 66.60° (440) of γ-Al_2O_3, while only the broad peak 2θ = 22° characteristic of silica was observed. Only for the SiO_2-based catalyst, a broad low-intensity reflex was observed at 2θ=44.35° that corresponds to (111) crystal plane of the metallic Co phase in the Fm-3m cubic unit cell (JCPDS Card No. 15–0806) [23]. Performing structural refinement did not provide information on the metal size due to the high dispersion of the metallic phases at the surface of the support.

Table 1. The main physico-chemical properties of the Ni-Co catalysts (reduced at 500°C).

Catalyst	BET surface area [m^2/g]	Pore volume [cm^3/g]	Average pore size [nm]	Acidity [µmol/g]
1%Ni-4%Co/TiO_2	40	0.36	15.1	256
1%Ni-4%Co/SiO_2	374	0.80	2.9	110
1%Ni-4%Co/Al_2O_3	145	0.22	2.5	663
4%Co/Al_2O_3	138	0.23	2.5	511
1%Ni/Al_2O_3	135	0.25	2.6	315

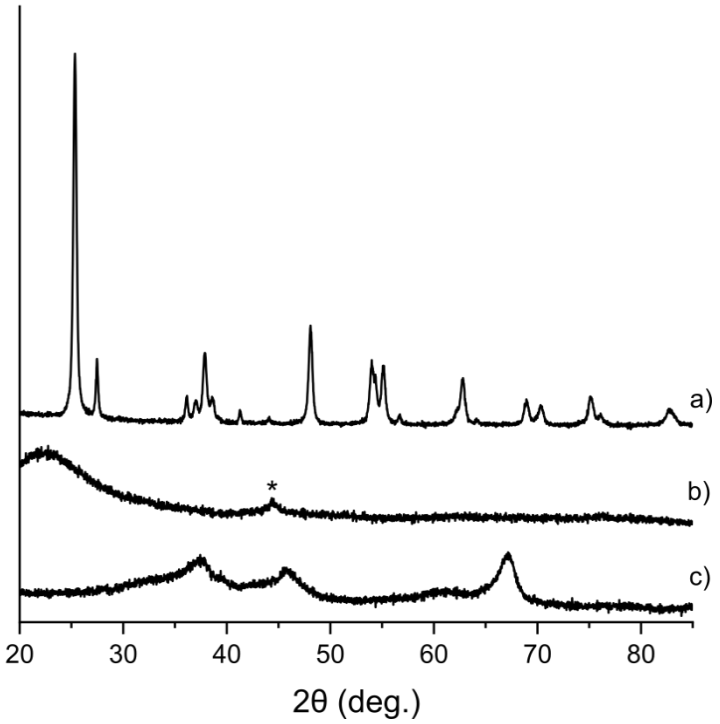

Figure 1. Powder XRD patterns of Ni-Co catalysts supported on a) TiO_2, b) SiO_2 and c) Al_2O_3 after the reduction step at 500°C. The asterisk marks the main peak attributed to metallic Co.

The catalysts differ in terms of specific surface area as well as of both size and volume of pores, surface acidity and reducibility of the supported metallic active phase. The Ni-Co/SiO_2 catalyst exhibited the highest specific surface area (374 m^2/g), while the catalysts based on γ-Al_2O_3 and TiO_2 displayed lower surface areas at 135-145 m^2/g and 40 m^2/g, respectively. The

209 SiO_2-based catalyst had the highest pore volume, associated to its highest specific surface area,
210 while the Al_2O_3-based catalysts displayed the lowest pore volume among the investigated
211 systems, both having similar mean pore sizes of 2-3 nm, in agreement with the literature
212 [24,25]. The TiO_2-based catalyst exhibited a relatively high pore volume in view of its low
213 surface area of 40 m^2/g, what is classically related to the inter-particle mesoporosity within
214 particle agglomerates, with a large pore size of 15 nm [26,27], TiO_2 P25 being a non-porous
215 material.

216 The number of surface acid sites present in the Ni-Co catalysts on the different supports
217 was determined through NH_3-TPD analysis (Figure S1). It is worth noting that the analysis of
218 the acidity of the catalysts comprises and includes as well that of the acidity of the supports
219 themselves. According to the literature data, both TiO_2 and Al_2O_3 supports, exhibit a similar
220 number of Lewis acid sites at the surface. However, TiO_2 and Al_2O_3 differ as being
221 characterized by weak and strong Lewis acid sites, respectively [28,29]. In the case of TiO_2,
222 Lewis acidity is related to the presence of Ti^{4+} ions at the support surface, while it results from
223 the presence of Al^{3+} sites in octahedral and tetrahedral symmetries for Al_2O_3 [30]. With regards
224 to SiO_2, the Lewis acidity remains negligible [31]. It should be mentioned that both Al_2O_3 and
225 SiO_2 supports are exposing Bronsted acid sites on their surface, which are related to the
226 presence of surface hydroxyl groups. However, the high-temperature treatment applied upon
227 the measurement dehydrates the surface, with the condensation of neighboring surface hydroxyl
228 groups therefore decreasing the contribution of Bronsted acidity. The presence of strong acid
229 sites of Lewis and Bronsted on the surface of catalysts is an important factor influencing
230 catalytic activity. However, the strength of the acid sites can be strongly influenced by the
231 presence of other species or catalysts preparation conditions.

232 The addition of transition metals to the above-mentioned supports influenced the acidity
233 of the catalysts. The lowest acidity was observed for the Ni-Co catalyst based on SiO_2 (110

μmol/g), and the highest one for the catalyst based on Al_2O_3 (663 μmol/g), while the Ni-Co/TiO_2 catalyst displayed an intermediate acidity at 256 μmol/g. It is worth adding that additional acid sites can be created as a result of metal-support interactions [24]. The presence of Ni or Co may cause an increase in acidity through to the creation of weak Bronsted acid sites [32,33]. Bridging hydroxyl groups can be created between the cation and the support surface [31]. In the case of Ni/Al_2O_3 and Co/Al_2O_3 catalysts, the presence of a strong metal-support interaction or the formation of a spinel may lead to an increase in acidity and acid strength. It is associated with an increase in the positive net charge or coordination of the unsaturated sites on the surface [32,33,34]. Also, the synergistic interaction between these two metals can significantly influence the distribution of acid sites in the bimetallic catalyst, as it is noteworthy that the acidity of the Ni-Co catalyst exceeded that of both monometallic counterparts.

The TPR profiles of the different catalysts after the calcination step are illustrated in Figure 2. The profile recorded for the monometallic Co/Al_2O_3 catalyst showed a first reduction peak between 300°C and 470°C and a second broad peak over the 500-700°C range, corresponding to the reduction of Co_3O_4 to CoO and CoO to Co^0 respectively [18,35]. The high temperature reduction effect could be also associated with the presence of interfacial $CoAl_2O_4$ phase. No clear reduction peak was observed for the monometallic nickel catalyst due to the low metal content. Ni is known to strong interact with the Al_2O_3 support and the NiO_x reduction might occur with the formation of a spinel interfacial phase [36] which usually is hardly visible during the TPR measurements, especially a low metal loading [36]. In regard of the Ni-Co bimetallic catalysts, the nature of the supports strongly impact the TPR profiles. It is worth noting that the bimetallic Ni-Co catalysts supported on Al_2O_3 exhibited a TPR profile analogous to that of the monometallic Co catalyst. A slight shift towards lower temperature was however observed for the low-temperature peak, that can be related the existence of strong Ni-Co interactions whereas effects at high temperature (450-700°C) could be related with Co or Ni

strong interaction with the support with possible formation of intermetallic species [37,38,39]. For the other bimetallic catalysts, the nickel and cobalt species were completely reduced at the temperature of 500°C. On the TiO_2 support, two broad and overlapping reduction peaks were recorded in the temperature range of 250-500°C. These peaks can be attributed to the simultaneous (multi-step) reduction of Co_3O_4 and NiO [40,41]. On SiO_2, three clear reduction peaks were observed at relatively low temperature in comparison to those recorded on both TiO_2 and Al_2O_3 counterparts, which suggests a limited interaction of the supported metallic phase with the support. The first effect at low temperature (180-250°C) could be related to the reduction of Co_3O_4 to CoO, while both second and third reduction peaks within the 250-400°C temperature range can be attributed to the simultaneous reduction of NiO and CoO [42]. .

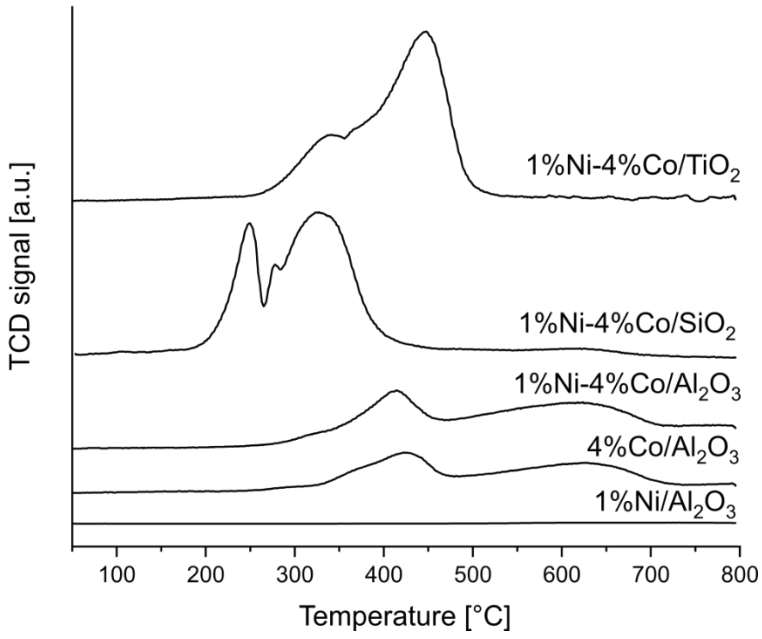

Figure 2. TPR profiles of the Ni-Co catalysts supported on TiO_2, SiO_2 and Al_2O_3 after the oxidation step at 500°C. The profiles of the Ni and Co monometallic counterparts on the Al_2O_3 support are reported for comparison.

XPS and time-of-flight secondary ion mass spectrometry (ToF-SIMS) analyses were performed for getting information about the catalyst surface and for identifying what kind of surface species were present, as well as their effect on the interactions between the metal(s) and the support (Tables 2 and 3). In regards to the XPS analysis, it must be said that metallic Co and Ni are known to undergo surface oxidation very easily when exposed to air, so that the XPS spectra of the Co 2p3/2 and Ni 2p3/2 orbitals exhibited only a broad envelope assigned to the core level peaks of Co or Ni species in oxidized state and to the usual shake-up satellite peak at higher binding energy, characteristic of Co or Ni species in oxidized states (not shown). However, surface atomic ratios were by far more informative. Comparing the catalysts on Al_2O_3 reduced at 500°C, the presence of Co favored a better dispersion of the Ni atoms at the support surface in the bimetallic NiCo catalyst in comparison to its monometallic counterpart, as evidenced by a higher Ni/Al surface atomic ratio of 0.050 vs. 0.025. Taking into account the high Ni/Co surface atomic ratio of 0.79 largely overcoming the bulk (nominal) value of 0.25 (1%Ni-4%Co), this might suggest an over-concentration of Ni at the surface of the NiCo nanoparticles, in agreement with the slight decrease in the Co/Al surface atomic ratio from 0.078 to 0.063. By contrast lower Ni/Co surface atomic ratios were obtained for NiCo catalysts on SiO_2 and TiO_2, suggesting that no Ni overconcentration was observed.

Table 2. Ni/Al, Co/Al and Ni/Co surface atomic ratios derived from XPS for the mono- and bi-metallic catalysts reduced at 500°C, except when directly specified.

Catalyst	Ni/Al	Co/Al	Ni/Co
1%Ni-4%Co/TiO_2	-	-	0.20
1%Ni-4%Co/SiO_2	-	-	0.12
4%Co/Al_2O_3	-	0.078	-
1%Ni/Al_2O_3	0.025	-	-
1%Ni-4%Co/Al_2O_3 (red. 300°C)	0.028	0.082	0.33
1%Ni-4%Co/Al_2O_3 (red. 500°C)	0.050	0.063	0.79
1%Ni-4%Co/Al_2O_3 (red. 650°C)	0.013	0.072	0.19

298 **Table 3.** Normalized intensity of selected ions identified on the surface of the 1%Ni-4%Co
299 catalysts and of the monometallic counterparts based on Al_2O_3 (reduced at 500°C).
300

	Selected ions Identified on the catalyst surface			
Catalyst	Ni^+ /total x10^{-3}	Co^+ /total x10^{-2}	$NiCoO_3H^-$ /total x 10^{-4}	Ni^+/Co^+
Ni-Co/TiO_2	0.93	1.17	4.56	0.81
Ni-Co/SiO_2	2.47	2.50	18.02	0.99
Ni-Co/Al_2O_3	6.30	1.42	5.29	4.44
Co/Al_2O_3	-	11.18	-	-
Ni/Al_2O_3	0.63	-	-	-

301

302 Those results were confirmed by ToF-SIMS analysis. The intensity of the Ni^+ ion was the
303 highest for the NiCo catalyst supported on Al_2O_3 among the different supports. Also the
304 bimetallic NiCo/Al_2O_3 catalyst exhibited a Ni^+ ion intensity higher by an order of magnitude
305 (6.3 vs. 0.63) compared to the monometallic Ni counterpart, what was in agreement with a high
306 dispersion of this metal on the catalyst surface, overcoming that of the monometallic catalyst.
307 Also the bimetallic catalyst on Al_2O_3 exhibited the highest intensity for the Ni^+/Co^+ ratio, in
308 agreement with an over-concentration of Ni at the surface of NiCo nanoparticles on Al_2O_3. By
309 contrast, the Co^+ ion intensity was strongly lower in the case of the bimetallic NiCo catalyst on
310 Al_2O_3 compared to its monometallic counterpart, what can correlate with a surface Ni
311 overconcentration, and can also result from the emergence of the $NiCoO_3H^-$ ion, which
312 indicates a significant interaction between the two metals. Similar Ni-Co interaction was
313 observed in NiCo on TiO_2, but the highest intensity of the $NiCoO_3H^-$ ion was observed on SiO_2,
314 what suggests either a stronger interaction or that the majority of Ni and Co atoms are in
315 interaction.

316

317 **3.2.Catalytic activity**

318

319 Table 4 shows the performances of the different Ni-Co catalysts in the GVL
320 hydrogenation reaction. The Ni-Co catalyst supported on Al_2O_3 clearly outperformed its

counterparts based on TiO_2 and SiO_2, in terms of both conversion and selectivity to 2-MTHF, and therefore of 2-MTHF yield. In the case of the catalysts supported on TiO_2 and Al_2O_3, the main reaction product was 2-MTHF. The highest yield to 2-MTHF (80%) was obtained with the 1%Ni-4%Co/Al_2O_3 catalyst, which was twice as high that on its TiO_2. In supported counterpart, together with the highest GVL conversion at 86%, vs. 53% on TiO_2. By contrast, the 1%Ni-4%Co/SiO_2 catalyst, led to the lowest selectivity to 2-MTHF, both 1,4-pentanediol and 2-MTHF reaction products were obtained , with the highest yield to 1,4-PDO of 43% and an intermediate conversion of 67%.

Table 4. Activity of the Ni-Co catalysts supported on TiO_2, SiO_2, Al_2O_3 (reduced at 500°C) in the GVL hydrogenation in terms of yields to the different products, GVL elimination, GVL conversion and carbon imbalance.

Catalyst	Product yield [%]						GVL elimination [%]	GVL conversion [%] [a]	Carbon imbalance [%] [b]
	2-MTHF	BuOH	2-PeOH	1-PeOH	VA	1,4-PDO			
1%Ni-4%Co/TiO_2	43	0	0	3	1	5	89	52	37
1%Ni-4%Co/SiO_2	20	3	0	0	1	43	73	67	6
1%Ni-4%Co/Al_2O_3	80	6	0	0	0	0	93	86	7
4%Co/Al_2O_3	46	1	1	3	0	1	84	52	32
1%Ni/Al_2O_3	0	1	0	0	1	1	31	3	28

Reaction conditions: 230°C; 5h; 0.6 g of catalyst, 1 g GVL; 30 ml 1,4-dioxane and 50 bar H_2

[a] the GVL conversion is expressed as the sum of the different yields

[b] calculated as the difference between the GVL elimination and the sum of the different product yields

In order to assess the influence of individual metals on the catalytic performances, the activity of the monometallic counterparts are also reported in Table 2 in the case of the Al_2O_3 support. The Ni catalyst showed no activity, while the Co catalyst was selective for 2-MTHF,

but with a GVL conversion of 52% being by far lower than that obtained with the Ni-Co system, giving a 46% 2-MTHF yield.

It is worth noting that a carbon imbalance was observed whatever the catalyst tested, as the sum of yields was not matching with the observed deficit in the GVL substrate (non-closure of the carbon balance). Indeed, the sum of the different product yields remained lower than the level of GVL elimination, with mismatch values ranging from 6% to 37% depending on the catalyst. Among the catalysts, the greatest carbon imbalances were observed for the catalyst based on titanium oxide and for monometallic catalysts. The smallest mismatch was obtained for the alumina-based catalyst giving the highest yield to MTHF and for the silica-based catalyst giving the highest yield to 1,4-PDO.

This carbon imbalance observed with different extents depending on the catalyst, was proposed to result from the adsorption of non-reacted GVL substrate at the catalyst surface, rather than the storage of reaction intermediates bound to the catalyst surface. Indeed, after cleaning the surface of the tested catalysts by dioxane, only traces of the GVL reactant were detected by HPLC analysis. Further, our previous works on Co/TiO_2 demonstrated that this carbon imbalance can be reduced by prolonging the reaction time with the consequent increase in the yield to 2-MTHF [15].

To this end, Table 5 and related Figure 3 summarize the influence of the reaction time on the activity of the $1\%Ni\text{-}4\%Co/Al_2O_3$. Regardless the reaction time, the progress of the reaction was characterized by its selectivity to 2-MTHF as main product. It is worth noting that already after 2 h of reaction almost complete GVL elimination was observed (90%), but associated to a high carbon imbalance. Prolonging the reaction time till 6 h reduced gradually the carbon imbalance observed and favours the further conversion of adsorbed (non-reacted) GVL into 2-MTHF, in consequence increasing the GVL conversion while keeping the same GVL

elimination. An almost complete conversion of the substrate was therefore obtained for a reaction time of 5-6 h, with a carbon imbalance close to zero.

Table 5. Influence of the reaction time on the catalytic activity of the 1%Ni-4%Co/Al_2O_3 catalyst in the GVL hydrogenation in terms of yields to the different products, GVL elimination and carbon imbalance.

Reaction time [h]	Product yield [%]						GVL elimination [%]	GVL conversion [%] [a]	Carbon imbalance [%] [b]
	2-MTHF	BuOH	2-PeOH	1-PeOH	VA	1,4-PDO			
1	10	1	0	0	1	2	47	14	33
2	43	1	0	2	0	4	90	50	40
3	53	1	0	3	0	4	90	61	29
4	55	5	0	6	0	10	92	76	16
5	80	6	0	0	0	0	93	86	7
6	78	2	1	5	0	5	93	91	2

Reaction conditions: 230°C; 5 h; 0.6 g of catalyst, 1 g GVL; 30 ml 1,4-dioxane and 50 bar H_2; reduction temperature: 500°C

[a] the GVL conversion is expressed as the sum of the different yields
[b] calculated as the difference between the GVL elimination and the sum of the different yields

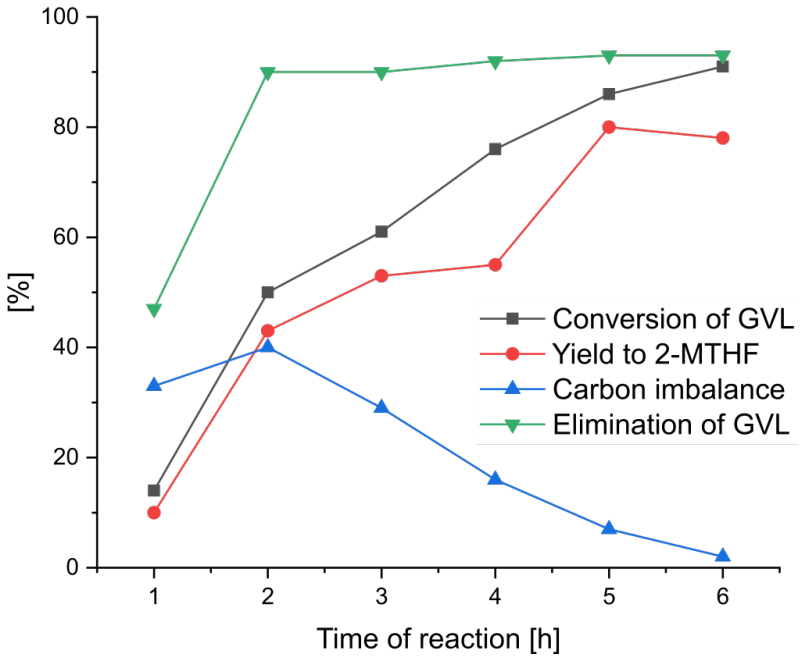

Figure 3. Influence of the time reaction on the GVL elimination, the GVL conversion, the yield to 2-MTHF and the carbon imbalance obtained with the 1%Ni-4%Co/Al_2O_3 catalyst.

This was also in line with the findings of Huang et al. [43] which found that the adsorption of the GVL substrate in the presence of a nonpolar solvent of the hydrocarbon type, occurs mainly on the oxide support and not on the metal sites in the case of a Ni-Cu/Al_2O_3 catalyst. They showed further that the 2-MTHF product was less prone to adsorb than the GVL reactant due to polarities and structural differences, in agreement with DFT calculations. They proposed that the stabilization of the hydrogen bond interaction between the hydroxyl H atom of the Al_2O_3 surface and the carbon oxygen atom of GVL contributes to the highest adsorption energy of GVL.

The differences observed in terms of carbon imbalance can in consequence be explained by differences in terms of the GVL adsorption rate on the surface of the catalysts that exhibited different surface properties.

This substantiates why the GVL conversion is expressed preferably as the sum of the yields to the different products. The decrease in GVL observed in our reaction conditions cannot be fully ascribed to the GVL conversion, and was labelled as GVL elimination, as it also comprises the GVL that remained adsorbed at the support surface.

3.3.Influence of synthesis parameters

XPS and ToF-SIMS were used to get information on the influence of the reduction temperature (300-650°C) on the surface features of the 1%Ni-4%Co/Al_2O_3 catalyst (Tables 2 and 6). These temperatures were selected on the basis of the TPR profiles (shown in Figure 2). Surface atomic ratio analysis revealed that low reduction temperature of 300°C did not change the surface availability of both Ni and Co species, with values similar to the corresponding monometallic catalysts, and a Ni/Co surface ratio close to the bulk nominal value. At the high temperature of 650°C, the Ni/Al surface ratio strongly dropped down from 0.050 for the catalyst

reduced at 500°C with surface over-concentration of Ni, to 0.013. This was accompanied by a strong decrease in the Ni/Co surface ratio from 0.79 to 0.19. This suggested a strongly lower availability of the Ni species at the surface of the bimetallic NiCo catalyst.

Table 6. Normalized intensity of selected ions identified on the surface of the 1%Ni-4%Co/Al_2O_3 catalysts as a function of the reduction temperature.

Reduction temperature	Ions Identified on the catalyst surface			
	Ni^+ /total x10^{-3}	Co^+ /total x10^{-2}	$NiCoO_3H^-$ /total x 10^{-4}	Ni^+/Co^+
300	7.00	0.92	3.76	7.61
400	6.93	1.16	5.05	5.97
500	6.30	1.42	5.29	4.44
650	2.71	0.68	7.68	3.99

In regards of ToF-SIMS, the intensity of the nickel ion on the surface decreased, as well as that of Ni^+/Co^+, while the intensity of Co^+ ions showed a volcano-like pattern. This decreasing trend does not reflect the over-concentration of Ni at the surface of the NiCo catalyst when increasing the reduction temperature to 500°C, as simultaneously was observed an increase in the intensity of the $NiCoO_3H^-$ ion, that materialized the interaction between both metals. The low value obtained at the high temperature reduction of 650°C for both Ni^+ and Co^+ ion intensities can be explained by the formation of a strong interaction between the two metals. In agreement with the increase in the intensity of the $NiCoO_3H^-$ ion.

Table 7 and the associated Figure 4 show the effect of the reduction temperature on the activity of the 1%Ni-4%Co/Al_2O_3 catalyst. For comparison the catalyst was also tested without reduction under H_2, i.e. only after the calcination step, but it did not show any significant activity. Therefore, the reduction step is a pre-treatment necessary for the activation of the metal on the support. Independently of the reduction temperature the reaction was highly selective and the main reaction product was 2-MTHF. A volcano-like relationship was observed for the

419 catalyst performances in respect of the reduction temperature. When using a reduction
420 temperature of 400°C and 500°C, relatively similar product yields were obtained, 76% and
421 80%, respectively, with a GVL conversion of 86%. Using a lower or higher reduction
422 temperature resulted in lower conversions and 2-MTHF yields, the more pronounced decrease
423 being observed at the high temperature of 650°C, giving a low yield to 2-MTHF of 34%. This
424 could be due to lack of availability of Ni species, as well as sintering and extensive formation
425 of Ni-Co interaction.

426

427 **Table 7.** Influence of the reduction temperature on the catalytic activity of the 1%Ni-
428 4%Co/Al_2O_3 catalyst in the GVL hydrogenation expressed in terms of GVL conversion and
429 product yields.

Temperature of reduction [°C]	Product yield [%]						GVL conversion [%] [a]
	2-MTHF	BuOH	2-PeOH	1-PeOH	VA	1,4-PDO	
-	1	0	0	0	1	2	4
300	60	2	0	4	0	4	70
400	76	5	0	5	0	0	86
500	80	6	0	0	0	0	86
650	34	1	0	1	2	5	43

Reaction conditions: 230°C; 5h; 0.6 g of catalyst, 1 g GVL; 30 ml 1,4-dioxane and 50 bar H_2

[a] the GVL conversion is expressed as the sum of the different yields

430

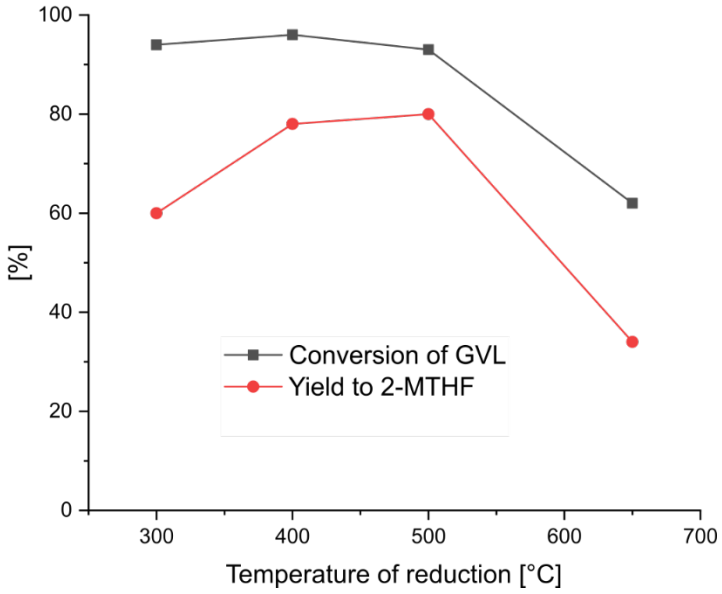

Figure 4. Influence of the reduction temperature on the GVL conversion and the yield to 2-MTHF obtained with the 1%Ni-4%Co/Al_2O_3 catalyst.

The Ni-Co ratio was the next parameter of interest to evaluate, while keeping constant at 5% the overall Ni-Co metal content. The results are summarized in Table 8. The 1%Ni-4%Co catalyst showed the highest GVL conversion and yield to 2-MTHF (80%). For other Ni and Co contents, strongly lower conversion and 2-MTHF yields were achieved, and similar yields to both main products (2-MTHF and 1,4-PDO) were obtained. Both GVL conversion and 2-MTHF yield showed a volcano-type relationship in respect of the Ni:Co ratio. In particular for monometallic 4%Ni nearly no activity was shown. It can be also observed that the presence of Co is favoring the selectivity to 2-MTHF. The addition of a small amount of Ni to Co is helping to boost the activity, while however a too high Ni content is negative to conversion and is orientating the selectivity of the reaction to 1,4-PDO.

449 **Table 8.** Influence of the Ni-Co metal ratio on the catalytic activity of the Ni-Co/Al_2O_3 catalyst
450 in the GVL hydrogenation in terms of GVL conversion and product yields.

Catalysts	Product yield [%]						GVL conversion [%] [a]
	2-MTHF	BuOH	2-PeOH	1-PeOH	VA	1,4-PDO	
4%Co	46	1	1	3	0	1	52
1%Ni-4%Co	80	6	0	0	0	0	86
2.5%Ni-2.5%Co	18	2	0	0	2	16	38
4%Ni-1%Co	6	0	0	0	3	6	15
4%Ni	0	2	0	0	2	2	6

Reaction conditions: 230°C; 5 h; 0.6 g of catalyst, 1 g GVL; 30 ml 1,4-dioxane and 50 bar H_2

[a] the GVL conversion is expressed as the sum of the different yields

451

452 **3.4. Catalyst reusability**

453 Reusability experiments were performed with the 1%Ni-4%Co/Al_2O_3 catalyst reduced at
454 500°C. The results are shown in Table S2 and Figure 5. After the first cycle, there was a slight
455 decrease for both GVL conversion and yield to 2-MTHF, which dropped from 86% and 80%
456 to 76% and 65% respectively. In the following cycles, the catalyst was stable until the fifth
457 reaction cycle ant the yield to 2-MTHF remained constant over 60%. Additionally, no leaching
458 of neither Co nor Ni was observed to the rection mixture. It is worth noting that the reuse of the
459 catalyst did not require any additional high-temperature treatment.

460

461

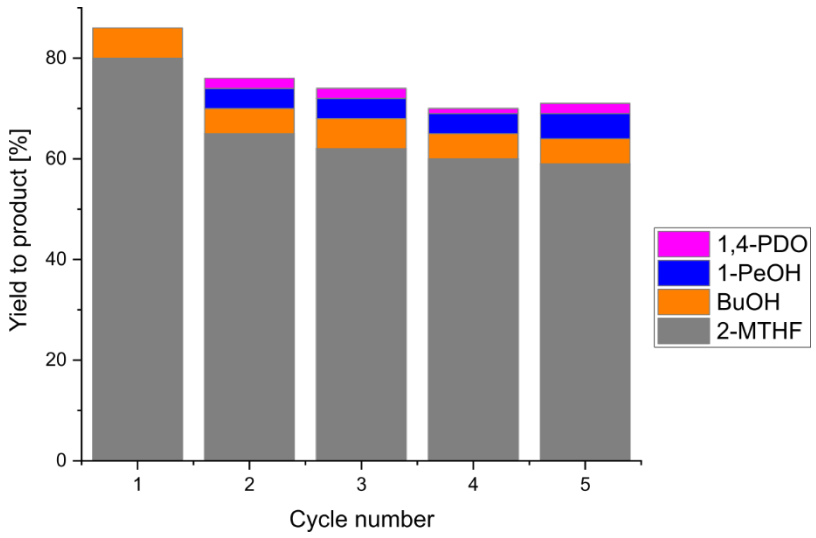

Figure 5. The recycling results for the 1%Ni-4%Co/Al_2O_3 catalyst (reduced at 500°C). Between each test cycle, the spent catalyst was washed in dioxane. Reaction conditions: 230°C; 5h; 0.6 g of catalyst, 1 g GVL; 30 ml 1,4-dioxane and 50 bar H_2.

3.5. Discussion

Our previous work showed the ability of earth-abundant non-noble metal Co catalysts to be used efficiently for the synthesis of MTHF from GVL [15]. Here, the activity of Ni-Co catalysts in the GVL hydrogenation reaction can be optimized through the use of an appropriate support, a suited Ni:Co ratio, as well as the selection of an adapted reduction temperature. We identified several key factors playing a role in the MTHF synthesis by Ni-Co catalysts.

The rate-determining reaction step in MTHF synthesis is the initial ring-opening of GVL hydrogenation that forms 1,4-PDO [44]. For this step, metal sites are necessary. The role of the metal can be discussed when comparing the performances of the catalysts on the same support, i.e. γ-Al_2O_3 catalyst, the activity of the bimetallic catalysts being much higher that obtained with their monometallic counterparts. Nearly no activity was even observed with the monometallic Ni catalyst. For the most active 1%Ni-4%Co/Al_2O_3 catalyst, the highest availability of Ni at the catalyst surface was observed while the existence of a Ni-Co interaction was demonstrated. We believe that both factors are of importance.

Although Ni alone is not showing any activity in the reaction, the addition Ni in appropriate amount to the Co catalyst allows the activity to be strongly boosted without any change in the selectivity to the targeted 2-MTHF product. We suggest that associating Ni in interaction with Co leads Ni to develop modified properties. We showed previously that the strong chemisorption of hydrogen taking place on pure Ni is significantly limiting the yield of hydrogenation reactions, whereas it was demonstrated that its alloying, for instance with Au, facilitates the hydrogenation by lowering the hydrogen poisoning effect [45]. This is also in agreement with the work of Dong et al. who reported a Ni-Co interaction under the form of a Ni-Co nanoalloy exhibiting a higher electron density that in consequence can promote the hydrogen activation and therefore facilitate the hydrogenation reaction in the case of d-glucose [16]. However, it must be said that optimal performances rely on an optimal reduction temperature. A minimum reduction temperature is necessary (>400-500°C), first to get complete reduction of the Ni species into metallic Ni, and second to involve large amount of Ni into the Ni-Co interaction. Indeed, although Ni is available in reasonable amount at the surface, low activity was observed. By contrast, a high reduction temperature boosted strongly the involvement of Ni atoms in Ni-Co interaction, but simultaneously limited the availability of Ni atoms at the surface.

Also the highest dispersion and therefore availability of Ni at the surface can be related with the existence of Ni-Co interactions. This was proposed by Li et al. [17] to be directly related to the formation of a spinel $NiCo_2O_4$ phase, that in appropriate amount can enhance the reducibility of Ni in the presence of Co, and favor the dispersion of both Ni and Co sites by inhibiting the crystallite growth at the support surface phases. In another work, this high dispersion was explained by the formation of a NiCo nanoalloy which was preventing nanoparticles to agglomerate [16].

We can also propose that the presence of adjacent nickel atoms in the Ni-Co systems might prevent the potential deposition of carbon over the cobalt sites as mentioned by Gonzalez de la Cruz et al. using Ni-Co/ZrO_2 catalysts [46]. This phenomena might be additionally strongly influenced by the Ni:Co ratio in the formed alloy [47].

The subsequent conversion of PDO towards MTHF is possible thanks to presence of acid sites, as they can catalyze the dehydration of the 1,4-PDO intermediate to 2-MTFH [48]. Therefore the presence of the acid sites can be considered as another crucial parameter. Indeed, in the case of NiCo catalysts supported on SiO_2 which are possessing the lowest acidity, a very low 2-MTHF production was observed, simultaneously to a significant yield to the 1,4-PDO intermediate. By contrast, nearly no 1,4-PDO production was observed using the catalyst supported on Al_2O_3, suggesting that the number of acid sites was sufficient for fastly converting the 1,4-PDO intermediate into 2-MTHF.

For Al_2O_3-based catalysts, that have an acidity within the 300-700 μmol/g range, a direct relationship was established, namely higher the acidity, higher the GVL conversion and yield to 2-MTHF (Figure 6). The weak and medium acid sites that most likely occur on Ni-Co/Al_2O_3 act as active sites and contribute to the hydrogenolysis of the C–O bond. This suggests that the acidity could be one of the limiting factors of the hydrogenation of GVL to 2-MTHF, in agreement with the literature [13].

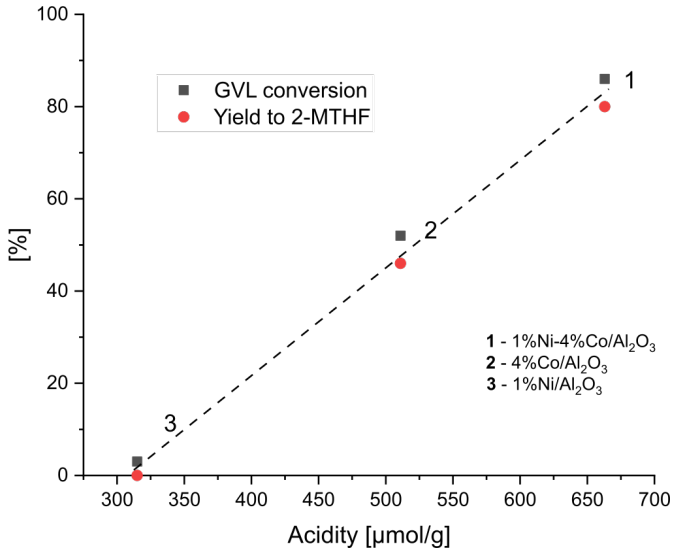

Figure 6. Influence of the surface acidity on both GVL conversion and yield to 2-MTHF obtained with the catalysts supported on γ-Al_2O_3.

We can further propose that a suited tuning of the features of the catalytic surface (e.g. availability of Ni and Co phases, potential interfacial spinel phase or NiCo nanoalloy, etc.) – that can be obtained by the modification of the synthesis parameters (notably reduction temperature and Ni:Co ratio) – might be an elegant way to influence directly the surface acidity of the catalyst, shown to be a key-factor necessary for achieving high performances.

4. CONCLUSIONS

In our work we demonstrated the ability of robust bimetallic Ni-Co catalysts to be active and selective towards 2-methyltetrahydrofuran which is considered as green fuel alternative. We investigated the influence of support, active phase composition and catalyst preparation conditions on the catalytic performances, as well as the catalyst reusability. Much higher yields to MTHF can be obtained on bimetallic Ni-Co catalysts than on the monometallic counterparts, the performance being however strongly depending on the ratio of the metals on the surface.

Monometallic Ni is nearly not active in the process, but its addition in appropriate amount to the Co catalyst strongly boosted the activity with high selectivity to the targeted 2-MTHF product. The Ni/Co surface ratio can be tuned by the reduction temperature which strongly influences the Ni dispersion and availability at the surface, with in consequence a remarkable enhancement of the catalytic performance. For optimum activity, reduction at 400-500°C is necessary to provide metallic Ni species, and to involve large amount of Ni into a beneficial Ni-Co interaction. Additionally, the acid sites have an important role to favor the dehydration of the 1,4-PDO intermediate to 2-MTFH. Only catalysts supported on alumina possessing acid sites in sufficient amount enabled to reach high yield 2-MTHF production.

ACKNOWLEDGEMENTS

The authors acknowledge gratefully the National Center of Science (NCN), Krakow, Poland, for financially supporting the work through a SONATA BIS grant (2016/22/E/ST4/00550). J. Rogowski (TUL) is thanked for performing ToF-SIMS measurements. V. Papaefthimiou (ICPEES) is thanked for performing XPS characterizations.

REFERENCES

[1] Li Y, Xu W, Jiang Y, Liew KM. Effects of diluents on laminar burning velocity and cellular instability of 2-methyltetrahydrofuran-air flames. Fuel 2022;308:121974. https://doi.org/10.1016/j.fuel.2021.121974.

[2] Wang J, Wang X, Fan X, Yang K, Zhang Y. An ignition delay time and kinetic study of 2-methyltetrahydrofuran at high temperatures. Fuel 2016;186:758–69. https://doi.org/10.1016/j.fuel.2016.08.104.

[3] Raj T, Chandrasekhar K, Banu R, Yoon J, Kumar G, Kim S. Synthesis of γ - valerolactone (GVL) and their applications for lignocellulosic deconstruction for sustainable green biorefineries. Fuel 2021;303:121333. https://doi.org/10.1016/j.fuel.2021.121333.

[4] Alonso DM, Bond JQ, Serrano-ruiz JC, Dumesic JA. Production of liquid hydrocarbon transportation fuels by oligomerization of biomass-derived C 9 alkenes 2010:992–9. https://doi.org/10.1039/c001899f.

[5] Adeleye AT, Louis H, Akakuru OU, Joseph I, Enudi OC, Michael DP. A Review on the conversion of levulinic acid and its esters to various useful chemicals. AIMS Energy 2019;7:165–85. https://doi.org/10.3934/ENERGY.2019.2.165.

[6] Leal Silva JF, Mariano AP, Maciel Filho R. Economic potential of 2-methyltetrahydrofuran (MTHF) and ethyl levulinate (EL) produced from hemicelluloses-derived furfural. Biomass and Bioenergy 2018;119:492–502. https://doi.org/10.1016/j.biombioe.2018.10.008.

[7] Pace V, Hoyos P, Castoldi L, María D De. 2-Methyltetrahydrofuran (2-MeTHF): A Biomass-Derived Solvent with Broad Application in Organic Chemistry 2012:1369–79. https://doi.org/10.1002/cssc.201100780.

[8] Ruppert AM, Grams J, Jędrzejczyk M, Matras-Michalska J, Keller N, Ostojska K, et al. Titania-Supported Catalysts for Levulinic Acid Hydrogenation: Influence of Support and its Impact on γ-Valerolactone Yield. ChemSusChem 2015;8:1538–47. https://doi.org/10.1002/cssc.201403332.

[9] Soszka E, Sneka-Płatek O, Skiba E, Maniukiewicz W, Pawlaczyk A, Rogowski J, Szynkowska-Jóźwik M, Ruppert AM, Influence of the presence of impurities and of the biomass source on the performance of Ru catalysts in the hydrolytic hydrogenation of cellulose towards γ-valerolactone, Fuel 2022;319:123646.

[10] Geilen FMA, Engendahl B, Harwardt A, Marquardt W. Selective and Flexible Transformation of Biomass-Derived Platform Chemicals by a Multifunctional Catalytic System. Angew Chemie 2010;49:5510–4. https://doi.org/10.1002/anie.201002060.

[11] Serrano-Ruiz JC, West RM, Dumesic JA. Catalytic conversion of renewable biomass resources to fuels and chemicals. Annu Rev Chem Biomol Eng 2010;1:79–100. https://doi.org/10.1146/annurev-chembioeng-073009-100935.

[12] Sun D, Saito T, Otsuka S, Ozawa T, Yamada Y, Sato S. Selective hydrogenation of γ-valerolactone to 2-methyltetrahydrofuran over Cu/Al2O3 catalyst. Appl Catal A Gen 2020;590:117309. https://doi.org/10.1016/j.apcata.2019.117309.

[13] Obregón I, Gandarias I, Ocio A, García-García I, Alvarez de Eulate N, Arias PL. Structure-activity relationships of Ni-Cu/Al2O3 catalysts for Γ-valerolactone conversion to 2-methyltetrahydrofuran. Appl Catal B Environ 2017;210:328–41. https://doi.org/10.1016/j.apcatb.2017.04.006.

[14] Novodárszki G, Solt HE, Valyon J, Lónyi F, Hancsók J, Deka D, et al. Selective hydroconversion of levulinic acid to γ-valerolactone or 2-methyltetrahydrofuran over silica-supported cobalt catalysts. Catal Sci Technol 2019;9:2291–304.

https://doi.org/10.1039/c9cy00168a.
[15] Emilia Soszka, Jędrzejczyk M, Lefèvre C, Ihiawakrim D, Keller N, Ruppert AM. TiO2-supported Co catalysts for the hydrogenation of γ-valerolactone to 2-methyltetrahydrofuran: influence of the support. Catal Sci Technol 2022. https://doi.org/doi.org/10.1039/D2CY01044E.
[16] Dong Q, Huang Y, Yang H, Pei J, Li K, Yuan M, et al. The Catalytic Hydrogenation of Biomass Platform Molecules by Ni–Co Nanoalloy Catalysts. Top Catal 2017;60:666–76. https://doi.org/10.1007/s11244-017-0774-4.
[17] Li S, Wang Y, Gao L, Wu Y, Yang X, Sheng P, et al. Short channeled Ni-Co/SBA-15 catalysts for highly selective hydrogenation of biomass-derived furfural to tetrahydrofurfuryl alcohol. Microporous Mesoporous Mater 2018;262:154–65. https://doi.org/10.1016/j.micromeso.2017.11.027.
[18] Yang P, Xia Q, Liu X, Wang Y. High-yield production of 2,5-dimethylfuran from 5-hydroxymethylfurfural over carbon supported Ni–Co bimetallic catalyst. J Energy Chem 2016;25:1015–20. https://doi.org/10.1016/j.jechem.2016.08.008.
[19] Kondeboina M, Enumula SS, Reddy KS, Challa P, Burri DR, Kamaraju SRR. Bimetallic Ni-Co/γ-Al2O3 catalyst for vapour phase production of γ-valerolactone: Deactivation studies and feedstock selection. Fuel 2021;285. https://doi.org/10.1016/j.fuel.2020.119094.
[20] Doniach S, Sunjic M. Many-electron singularity in X-ray photoemmision. J Phys C Solid State Phys 1970;3:285–91.
[21] Shirley DA. High-resolution x-ray photoemission spectrum of the valence bands of gold. Phys Rev B 1972;5:4709–14. https://doi.org/10.1103/PhysRevB.5.4709.
[22] Scofield JH. Hartree-Slater subshell photoionization cross-sections at 1254 and 1487 eV. J Electron Spectros Relat Phenomena 1976;8:129–37. https://doi.org/10.1016/0368-2048(76)80015-1.
[23] Cai P, Ci S, Zhang E, Shao P, Cao C, Wen Z. FeCo Alloy Nanoparticles Confined in Carbon Layers as High-activity and Robust Cathode Catalyst for Zn-Air Battery. Electrochim Acta 2016;220:354–62. https://doi.org/10.1016/j.electacta.2016.10.070.
[24] Raikwar D, Majumdar S, Shee D. Synergistic effect of Ni-Co alloying on hydrodeoxygenation of guaiacol over Ni-Co/Al2O3 catalysts. Mol Catal 2021;499:111290. https://doi.org/10.1016/j.mcat.2020.111290.
[25] Gai X, Yang D, Tang R, Luo M, Lu P, Xing C, et al. Preparation of Ni-Co/SiO2 catalyst by ammonia reflux impregnation and its CH4-CO2 reforming reaction performance. Fuel 2022;316:123337.
[26] Nu Hoai Nguyen V, Amal R, Beydoun D. Photocatalytic reduction of selenium ions using different TiO2 photocatalysts. Chem Eng Sci 2005;60:5759–69. https://doi.org/10.1016/j.ces.2005.04.085.
[27] Alonso-Tellez A, Masson R, Robert D, Keller N, Keller V. Comparison of Hombikat UV100 and P25 TiO 2 performance in gas-phase photocatalytic oxidation reactions. J Photochem Photobiol A Chem 2012;250:58–65. https://doi.org/10.1016/j.jphotochem.2012.10.008.
[28] Hirotoshi N. Properties of acid sites on TiO2-SiO2 and TiO2-Al2O3 mixed oxides measured by infrared spectroscopy. Bull Chem Soc Jpn 1992;65:914–6.
[29] Massa M, Andersson A, Finocchio E, Busca G. Gas-phase dehydration of glycerol to acrolein over Al2O 3-, SiO2-, and TiO2-supported Nb- and W-oxide catalysts. J Catal 2013;307:170–84. https://doi.org/10.1016/j.jcat.2013.07.022.
[30] Zaki MI, Hasan MA, Al-sagheer FA. In situ FTIR spectra of pyridine adsorbed on SiO 2 – Al 2 O 3 , TiO 2 , ZrO 2 and CeO 2 : general considerations for the identification of acid sites on surfaces of finely divided metal oxides 2001;190:261–74.

[31] Connell G, Dumesic JA. The generation of Brønsted and Lewis acid sites on the surface of silica by addition of dopant cations. J Catal 1987;105:285–98. https://doi.org/10.1016/0021-9517(87)90059-5.
[32] Stanislaus A, M. A-H, K. A-D. Effect of Nickel on the Surface Acidity of Molybdenum Hydrotreating Catalysts. Appl Catal 1989;50:237–45.
[33] de Bokx PK, Wassenberg WBA, Geus JW. Interaction of nickel ions with a γ-Al2O3 support during deposition from aqueous solution. J Catal 1987;104:86–98. https://doi.org/10.1016/0021-9517(87)90339-3.
[34] Dewangan N, Ashok J, Sethia M, Das S, Pati S, Kus H, et al. Cobalt-Based Catalyst Supported on Different Morphologies of Alumina for Non-oxidative Propane Dehydrogenation: Effect of Metal Support Interaction and Lewis Acidic Sites. ChemCatChem 2019;11:4923–34. https://doi.org/10.1002/cctc.201900924.
[35] Liu P, Sun L, Jia X, Zhang C, Zhang W, Song Y. Efficient one-pot conversion of furfural into 2-methyltetrahydrofuran using non-precious metal catalysts. Mol Catal 2020;490:110951. https://doi.org/10.1016/j.mcat.2020.110951.
[36] Soszka E, Reijneveld HM, Jędrzejczyk M, Rzeźnicka I, Grams J, Ruppert AM. Chlorine Influence on Palladium Doped Nickel Catalysts in Levulinic Acid Hydrogenation with Formic Acid as Hydrogen Source. ACS Sustain Chem Eng 2018;6:14607–13. https://doi.org/10.1021/acssuschemeng.8b03211.
[37] Pinilla JL, de Llobet S, Moliner R, Suelves I. Ni-Co bimetallic catalysts for the simultaneous production of carbon nanofibres and syngas through biogas decomposition. Appl Catal B Environ 2017;200:255–64. https://doi.org/10.1016/j.apcatb.2016.07.015.
[38] Konishcheva M V., Svintsitskiy DA, Potemkin DI, Rogozhnikov VN, Sobyanin VA, Snytnikov P V. Catalytic Performance and Characterization of Highly Efficient Composite Ni(Clx)/CeO2/η-Al2O3/FeCrAl Wire Mesh Catalysts for Preferential CO Methanation. ChemistrySelect 2020;5:1228–34. https://doi.org/10.1002/slct.201904630.
[39] Gebresillase MN, Raguindin RQ, Kim H, Seo JG. Supported bimetallic catalysts for the solvent-free hydrogenation of levulinic acid to γ-valerolactone: Effect of metal combination (ni-cu, ni-co, cu-co). Catalysts 2020;10:1–20. https://doi.org/10.3390/catal10111354.
[40] Takanabe K, Nagaoka K, Nariai K, Aika KI. Titania-supported cobalt and nickel bimetallic catalysts for carbon dioxide reforming of methane. J Catal 2005;232:268–75. https://doi.org/10.1016/j.jcat.2005.03.011.
[41] Nagaoka K, Takanabe K, Aika KI. Modification of Co/TiO2 for dry reforming of methane at 2 MPa by Pt, Ru or Ni. Appl Catal A Gen 2004;268:151–8. https://doi.org/10.1016/j.apcata.2004.03.029.
[42] Guo M, Lu G. The regulating effects of cobalt addition on the catalytic properties of silica-supported Ni–Co bimetallic catalysts for CO2 methanation. React Kinet Mech Catal 2014;113:101–13. https://doi.org/10.1007/s11144-014-0732-0.
[43] Huang YB, Liu AF, Zhang Q, Li KM, Porterfield WB, Li LC, et al. Mechanistic Insights into the Solvent-Driven Adsorptive Hydrodeoxygenation of Biomass Derived Levulinate Acid/Ester to 2-Methyltetrahydrofuran over Bimetallic Cu-Ni Catalysts. ACS Sustain Chem Eng 2020;8:11477–90. https://doi.org/10.1021/acssuschemeng.0c00335.
[44] Shao Y, Ba S, Sun K, Gao G, Fan M, Wang J, et al. Selective production of γ-valerolactone or 1,4-pentanediol from levulinic acid/esters over Co-based catalyst: Importance of the synergy of hydrogenation sites and acidic sites. Chem Eng J 2022;429:132433.

[45] Ruppert AM, Jędrzejczyk M, Potrzebowska N, Kaźmierczak K, Brzezińska M, Sneka-Płatek O, et al. Supported gold-nickel nano-alloy as a highly efficient catalyst in levulinic acid hydrogenation with formic acid as an internal hydrogen source. Catal Sci Technol 2018;8:4318–31. https://doi.org/10.1039/c8cy00462e.
[46] Gonzalez-Delacruz VM, Pereñiguez R, Ternero F, Holgado JP, Caballero A. In situ XAS study of synergic effects on Ni-Co/ZrO 2 methane reforming catalysts. J Phys Chem C 2012;116:2919–26. https://doi.org/10.1021/jp2092048.
[47] Bian Z, Kawi S. Highly carbon-resistant Ni-Co/SiO2 catalysts derived from phyllosilicates for dry reforming of methane. J CO2 Util 2017;18:345–52. https://doi.org/10.1016/j.jcou.2016.12.014.
[48] Huang Y, Liu A, Zhang Q, Li K, Porter WB, Li L, et al. Mechanistic Insights into the Solvent-Driven Adsorptive Hydrodeoxygenation of Biomass Derived Levulinate Acid/Ester to 2 - Methyltetrahydrofuran over Bimetallic Cu − Ni Catalysts. ACS Sustain Chem Eng 2020;8:11477–90. https://doi.org/10.1021/acssuschemeng.0c00335.

Supporting Information

High yield production of 2-methyltetrahydrofuran biofuel with reusable Ni-Co catalysts

Emilia Soszka[1], Marcin Jędrzejczyk[1], Nicolas Keller[2], Agnieszka M. Ruppert[1*]

[1] Institute of General and Ecological Chemistry, Lodz University of Technology, ul. Żeromskiego 116, 90-924 Łódź (Poland)

[2] Institut de Chimie et Procédés pour l'Energie, l'Environnement et la Santé, CNRS/University of Strasbourg, 67087 Strasbourg, France ; nkeller@unistra.fr

*Correspondence: agnieszka.ruppert@p.lodz.pl

Figure S1

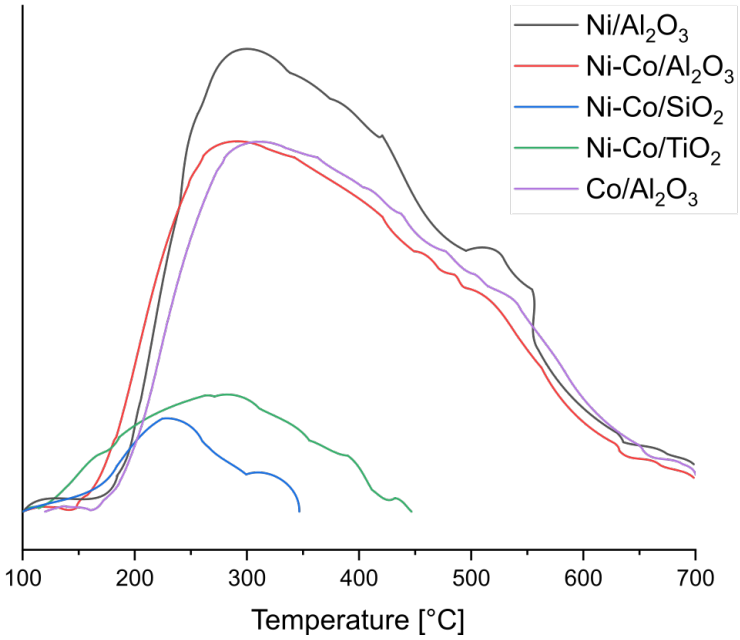

Figure S1. TPD-NH_3 profiles obtained for the investigated catalysts (reduced at 500°C).

Table S1. Comparison with the literature results

[1] Al-Shaal MG, Dzierbinski A, Palkovits R. Solvent-free γ-valerolactone hydrogenation to 2-methyltetrahydrofuran catalysed by Ru/C: A reaction network analysis. Green Chem 2014;16:1358–64. https://doi.org/10.1039/c3gc41803k.

[2] Licursi D, Antonetti C, Fulignati S, Giannoni M, Raspolli Galletti AM. Cascade strategy for the tunable catalytic valorization of levulinic acid and γ-valerolactone to 2-methyltetrahydrofuran and alcohols. Catalysts 2018;8:277. https://doi.org/10.3390/catal8070277.

[3] Obregón I, Gandarias I, Ocio A, García-García I, Eulate NA De, Arias PL. Applied Catalysis B : Environmental Structure-activity relationships of Ni-Cu/Al2O3 catalysts for gamma -valerolactone conversion to 2-methyltetrahydrofuran. "Applied Catal B, Environ 2017;210:328–41. https://doi.org/10.1016/j.apcatb.2017.04.006.

[4] Huang X, Kudo S, Ashik UPM, Einaga H, Hayashi J. Selective Hydrodeoxygenation of γ-Valerolactone over Silica- supported Rh-based Bimetallic Catalysts 2020:0–7. https://doi.org/10.1021/acs.energyfuels.0c01290.

Catalyst	Reaction	Reaction conditions	MTHF Yield [%]	Ref.
5%Ru/C	The reactions were performed in batch autoclave reactor.	GVL (3 g, 29.9mmol), 5%Ru/C (150 mg, 0.07 mmol of Ru), solvent free, pressure 100 bar H_2, temperature 190°C reaction time 24 h.	43	[1]
5%Ru/C, 10%Re/C catalysts, and zeolite HY as acid co-catalyst.	The reactions were carried out in a stainless steel, batch, mechanically stirred Parr autoclave.	GVL: 1.68 g; Ru: 2 mg (GVL/Ru: 847.63 mol/mol); NBP 500 mg, H_2O: 40 mL; P_{H2} : 9.0 MPa; temperature 200°C; reaction time 3 h.	35.7	[2]
5%Ru/C, 10%Re/C catalysts, and niobium phosphate as acid co-catalyst.	The reactions were carried out in a stainless steel, batch, mechanically stirred Parr autoclave.	GVL: 1.68 g; Ru: 2 mg (GVL/Ru: 847.63 mol/mol); HY zeolite: 500 mg, solvent -H_2O: 40 mL; PH_2 : 9.0 MPa, temperature 200°C reaction time 3 h.	64.9	[2]
Ni-Cu/Al_2O_3	Activity tests were carried out in Hastelloy autoclaves with a magnetic stirrer and a glass liner.	temperature 230◦C, 50 bar H_2 pressure, GVL-to-Cat. weight ratio of 10, 5 wt% GVL in 2-butanol as solvent, and 5 h reaction time.	55	[3]

4%RhMo/SiO_2 The molar ratio of Mo/Rh was 0.5	The reaction was conducted in a stainless steel autoclave	Reaction conditions: GVL, catalyst, solvent-heptane and H_2 pressure 4.5 MPa, temperature 120°C, reaction time 6 h,	65	[4]

Table S2. The recycling results for the 1%Ni-4%Co/Al_2O_3 catalyst (reduced at 500°C).

Number of cycle	Product yield [%]						GVL conversion [%] [a]
	2-MTHF	BuOH	2-PeOH	1-PeOH	VA	PDO	
1	80	6	0	0	0	0	86
2	65	5	0	4	0	2	76
3	62	6	0	4	0	2	74
4	60	5	0	4	0	1	70
5	59	5	0	5	0	2	71

Reaction conditions: 230°C; 5h; 0.6 g of catalyst, 1 g GVL; 30 ml 1,4-dioxane and 50 bar H_2, between each test cycle, the spent catalyst was washed in dioxane

[a] the GVL conversion is expressed as the sum of the different yields

[b] calculated as the difference between the GVL elimination and the sum of the different yields

Table S3. Relative intensity of the chosen ions identified on the 1%Ni-4%Co/Al_2O_3 catalysts surface by ToF-SIMS

1%Ni-4%Co/Al_2O_3	Relative intensity of the chosen ions identified on the catalysts surface to total ions observed.			
	Ni^+ x 10^{-3}	**Co^+ x 10^{-2}**	**CoO_2^- x 10^{-3}**	**Al^+ x 10^{-1}**
Fresh (reduced at 500°C)	6.3	1.4	2.8	1.04
After reaction (5h)	7.1	2.0	3.0	1.05

The relative intensity of the signals associated to Ni and Co species slightly increased after the reaction in comparison to the fresh catalyst. This effect was observed for both metals, so that it most probably resulted from the cleaning of the surface from some precursor residue in the reactional environment.

Another possible reason could be related to the surface migration of the metals in hydrothermal conditions under hydrogen pressure. However, this alternative explanation was discarded, as this phenomena is often associated with leaching, that was demonstrated not to occur in our reaction conditions